AUTOMATIC RADICLE LENGTH ESTIMATION OF GERMINATED CUCUMBER SEEDS BASED ON GERMHRNET

/

基于 GermHRNet 的发芽黄瓜种子胚根长度自动估测方法

Rui ZHAO[1)], Heng ZHAO[1)], Feng ZHANG[1)], Wenjie LI[2)], Bei WANG[2)], Qi WANG[4)], Yiting SU[1)], Qiulan WU[*1)], Bo ZHOU[*2,3)],

[1)]College of Information Science and Engineering, Shandong Agricultural University, Tai'an/China
[2)]College of Life Sciences, Shandong Agricultural University, Tai'an/China
[3)]Eukaryotic Biotechnology (Shandong) Co., Ltd., Tai'an/China
[4)]Yoheng Biotechnology (Ningbo) Co., Ltd., Ningbo/China
Corresponding author: Qiulan WU; Tel: +86 13181817575; E-mail: zxylsg@sdau.edu.cn
Bo ZHOU; Tel: +86 13562802798; E-mail: Zhoubo2798@163.com

DOI: https://doi.org/10.35633/inmateh-79-85

Keywords: *Cucumber seeds, Radicle length estimation, Keypoint detection, High-throughput plant phenotyping*

ABSTRACT

Radicle length is an important phenotypic trait for evaluating the growth-promoting effects of plant growth-promoting rhizobacteria on cucumber seeds. However, conventional manual measurement is time-consuming, labor-intensive, and prone to subjective errors, while existing radicle phenotyping systems still suffer from insufficient throughput. To address these limitations, this study proposes an automatic radicle length estimation method for germinated cucumber seeds based on GermHRNet. First, a YOLOv8-p2s model was used to automatically detect seed instances in Petri dish images. Subsequently, a GermHRNet keypoint detection network was developed to accurately localize radicle keypoints. A high-resolution cross-scale feature enhancement module and a dynamic coordinate feature enhancement module were introduced to improve feature representation and keypoint localization accuracy for slender and curved radicles. Finally, radicle length was estimated using a polyline-based pixel distance accumulation strategy according to the detected keypoint coordinates. Experimental results showed that the proposed method achieved an average precision, average recall, and percentage of correct keypoints of 90.6%, 92.2%, and 88.2%, respectively. The mean absolute error, root mean square error, normalized mean absolute error, normalized root mean square error, and coefficient of determination for radicle length estimation were 0.51 mm, 0.61 mm, 6.06%, 7.25%, and 0.98, respectively. Under a CPU-only environment without GPU acceleration, the proposed method achieved a throughput of 3.38 × 10^4 seeds/h. The proposed method enables rapid and accurate radicle length acquisition without specialized equipment and provides an efficient technical solution for large-scale microbial strain screening and seed phenotyping.

摘要

黄瓜种子胚根长度是评价植物促生根际菌促生效应的重要表型参数，但传统人工测量费时费力且主观性强，而现有胚根表型采集系统也存在通量不足的问题。为此，本研究提出一种基于 GermHRNet 的发芽黄瓜种子胚根长度自动估测方法。首先，利用 YOLOv8-p2s 模型实现培养皿中种子个体的自动检测。随后，构建 GermHRNet 关键点检测网络，实现胚根关键点的准确定位。通过引入高分辨率交叉特征增强模块和动态坐标特征增强模块，提高了细长弯曲胚根的特征表达与关键点定位精度。最后，基于关键点坐标采用多段折线像素距离累积方法实现胚根长度估测。结果表明：关键点检测的平均精度、平均召回率和正确关键点百分比分别达到 90.6%、92.2% 和 88.2%；长度估测的平均绝对误差、均方根误差、归一化平均绝对误差、归一化均方根误差和决定系数分别为 0.51 mm、0.61 mm、6.06%、7.25%和 0.98；在普通设备 CPU 推理且未启用 GPU 加速的环境下，单机处理通量可达 3.38×10^4 粒/h。该方法无需专业设备即可实现发芽黄瓜种子胚根长度的准确、快速获取，可为大规模菌株筛选及种子表型分析提供高效技术支撑。

INTRODUCTION

Cucumber is widely used as a representative crop for investigating root development in plant physiology and plant–microbe interaction studies because of its short growth cycle, clear phenotypic characteristics, and high sensitivity to environmental changes *(Shaik et al., 2025).* In studies involving plant growth-promoting rhizobacteria (PGPR), cucumber seeds are commonly used as experimental materials to evaluate the growth-promoting potential of microbial strains and their combinations *(Fu et al., 2026).* Radicle length is one of the most important phenotypic indicators of early root development, as it directly reflects seed germination status and the regulatory effects of microbial metabolites on root growth. However, PGPR screening usually requires the evaluation of a large number of candidate strains, which places high demands on both the efficiency and accuracy of radicle length measurement. At present, radicle length measurement still largely depends on manual operation, which is time-consuming, labor-intensive, and susceptible to subjective errors. Although several automated seed phenotyping systems, such as TPN-Pheno-ZM1 *(Top Cloud-Agri Technology Co., Ltd., 2026)* and OpenPheno *(Hu et al., 2025)*, have been developed to improve measurement efficiency, their throughput for radicle length measurement remains limited. For example, the TPN-Pheno-ZM1 system can process only approximately 1,000 seeds within 2 h. Therefore, developing an accurate, efficient method for automatic radicle length estimation is of practical importance for high-throughput microbial screening and seed phenotyping.

To realize automatic radicle length estimation in germinated seeds, image semantic segmentation has been widely used to extract radicle regions and estimate length based on contour or skeleton information *(Wu et al., 2024; Zhao et al., 2025)*. However, segmentation-based methods are highly dependent on image quality and segmentation accuracy. When radicles are curved, slightly lifted from the filter paper, adherent to the background, or partially blurred, these methods are prone to structural discontinuities, boundary errors, and mis-segmentation, which may further affect length estimation. Compared with segmentation-based methods, keypoint detection provides a more structured representation by localizing critical anatomical or morphological positions of the target *(Li et al., 2026).* This strategy reduces the dependence on complete pixel-level segmentation and can provide a more robust representation of complex radicle morphology. In recent years, keypoint detection has been increasingly applied to agricultural phenotyping tasks. For example, *Chen et al. (2025)* developed an improved LTHRNet model for accurate localization and pose estimation of pineapple fruit keypoints. *Yuan et al. (2026)* proposed CLR-YOLO-Pose based on YOLO-Pose, which improved keypoint detection performance under complex scenarios and enabled high-precision measurement of peduncle length. *He et al. (2024)* introduced DEKR-SPrior based on a bottom-up keypoint detection framework for phenotypic analysis of soybean pods in complex field environments. *Pan et al. (2025)* developed the PFLO model to reconstruct plant skeletons from keypoints for high-precision maize phenotyping. *Wu et al. (2023)* improved HRNet by incorporating a Ghost module and developed a lightweight keypoint detection model for grape stem recognition in complex cluster structures. *Niu et al. (2025)* introduced an attention mechanism into YOLOv11-Pose to achieve whole-plant keypoint localization and phenotypic parameter extraction in maize. *Chen et al. (2024)* improved skeleton extraction and phenotypic parameter acquisition for individual rice tillers by integrating the CBAM module into a cascaded pyramid network. These studies demonstrate the potential of keypoint detection for plant phenotyping. However, most existing methods focus on relatively large plant organs, such as fruits, stems, pods, tillers, or whole plants, which usually have more distinct structural features. In contrast, germinated seed radicles are small, slender, curved, and sometimes structurally discontinuous in images. As a result, keypoint detection for germinated seed radicles remains insufficiently investigated, and a dedicated methodological framework is still lacking.

In summary, automatic radicle length estimation still faces two main challenges. First, existing measurement methods often rely on manual operation, specialized imaging devices, or low-throughput processing workflows, making them difficult to apply to large-scale microbial strain screening. Second, current keypoint detection methods have limited capability in preserving fine structural details of small and slender targets, which may lead to unstable or inaccurate keypoint localization when radicles show obvious curvature, complex poses, adhesion to the filter paper, or blurred root tips.

To address these challenges, this study proposes a GermHRNet-based automatic radicle length estimation method for germinated cucumber seeds. Based on the high-resolution network (HRNet), the proposed method enhances the keypoint detection framework to improve the representation of fine radicle structures and the localization stability of curved radicles. Specifically, YOLOv8-p2s is first used to detect individual seed instances in Petri dish images. Then, GermHRNet is constructed to localize radicle keypoints accurately.

To improve the representation of slender radicle structures, a high-resolution cross-scale feature enhancement strategy was introduced. In addition, a coordinate-aware dynamic feature enhancement strategy was further incorporated to enhance spatial coordinate awareness and reduce keypoint displacement caused by radicle curvature. Finally, radicle length is estimated using a polyline-based pixel-to-millimeter accumulation method. The proposed method aims to provide an accurate, rapid, and high-throughput technical solution for cucumber seed radicle phenotyping and large-scale PGPR screening.

The main contributions of this study are summarized as follows:

1) An automated radicle phenotyping framework integrating seed detection, keypoint localization, and radicle length estimation was developed for germinated cucumber seeds, providing an efficient technical solution for large-scale PGPR screening.

2) A GermHRNet-based keypoint detection model was proposed to improve the localization accuracy of small, slender, and curved radicles. The model enhances fine-grained structural representation and spatial coordinate perception for complex radicle morphology.

3) A polyline-based radicle length estimation strategy was established to achieve accurate radicle length quantification without relying on pixel-level segmentation, thereby improving robustness under curved and partially blurred radicle conditions.

4) The proposed framework achieved accurate and high-throughput radicle phenotyping under CPU-only deployment conditions, demonstrating its practical potential for low-cost agricultural phenotyping applications.

MATERIALS AND METHODS

Data Acquisition and Dataset Construction

High-Throughput Image Acquisition System

To satisfy the requirements for high-quality and large-scale image acquisition in radicle phenotyping, a high-throughput imaging system for germinated seeds was designed and developed in this study, as shown in Fig. 1. The system consisted of three main modules: image acquisition, image processing, and data management.

Fig. 1 - High-throughput image acquisition system for germinated seeds

For image acquisition, the system consisted of an industrial camera produced by Jierui Weitong Co., Ltd., China, an aluminum-alloy frame, and a standardized Petri dish holder. Images were acquired at a resolution of 1600 × 1200 pixels. During image acquisition, the vertical distance between the camera lens and the Petri dish plane was fixed at 42 cm to ensure consistent imaging conditions. The holder accommodated up to 12 Petri dishes with a diameter of 9 cm in a single acquisition, allowing batch image acquisition. A reference ruler was placed in the imaging plane for scale calibration, and the calibrated scale factor was approximately 6 pixels/mm. This scale factor was used to convert the estimated radicle length from pixel units to physical length.

For image processing, the system provided basic preprocessing functions. Original images containing multiple Petri dishes were automatically divided into individual dish images. In addition, image parameters such as brightness, sharpness, and resolution could be adjusted to improve image consistency and reduce quality differences among samples. These preprocessing procedures provided standardized data for subsequent seed detection, keypoint localization, and radicle length estimation.

For data management, the system supported centralized storage and standardized organization of acquired images and related experimental data. This facilitated dataset construction, sample retrieval, and subsequent model training and evaluation.

The developed imaging system provided a standardized and efficient platform for high-throughput radicle phenotyping of germinated cucumber seeds.

High-Throughput Image Acquisition

The cucumber seeds used in this study were from the cultivar Zhongnong No. 6 and were provided by the State Key Laboratory of Crop Biology at Shandong Agricultural University. Before the germination experiment, healthy, well-filled, and morphologically uniform seeds were manually selected to reduce the influence of seed quality variation on radicle phenotyping. The selected seeds were placed in standard Petri dishes with a diameter of 9 cm and incubated in a constant-temperature incubator at 25 °C under dark conditions for 48 h. After germination, seed images were acquired using the custom-built high-throughput image acquisition system shown in Fig. 1. Each original image contained 12 Petri dishes, as illustrated in Fig. 2, and the average acquisition time for one original image was approximately 0.35 s. A total of 220 original images were collected, including 2,640 Petri dishes and 34,793 germinated cucumber seeds. These images were used for subsequent seed detection, radicle keypoint annotation, model training, and radicle length estimation.

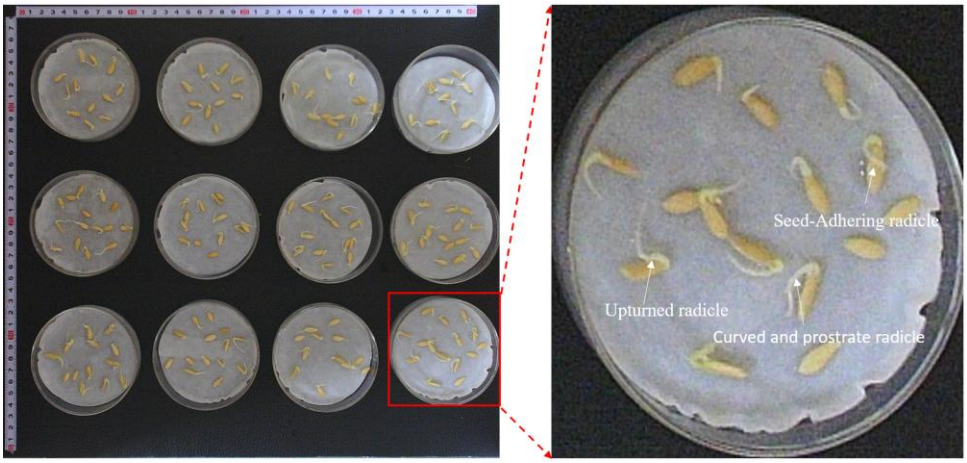

Fig. 2 - Images of germinated cucumber seeds

Dataset Construction

After image acquisition, the 220 original images were divided into two datasets: CucumberSeeds-1 and CucumberSeeds-2. CucumberSeeds-1 contained 100 original images with 15,653 seeds and was used for model training, validation and testing. The dataset was divided into training, validation and test sets at a ratio of 8:1:1. Since each original image contained 12 Petri dishes and a large number of seed instances, an automatic cropping procedure was used to convert the original multi-dish images into single-dish images. This operation increased the effective number of samples and provided clearer local image information for fine-grained radicle feature learning. After cropping, the dataset included 960 training images, 120 validation images and 120 test images. CucumberSeeds-2 contained 120 original images with 19,140 seeds and was used to evaluate the high-throughput phenotyping performance of the proposed method.

The LabelMe annotation tool was used to construct the radicle keypoint dataset. Each seed was annotated with a bounding box and four radicle keypoints, namely the radicle base, pre-bending point, post-bending point and root tip. As shown in Fig. 3, the four-keypoint annotation scheme was determined through preliminary experiments. When fewer than four keypoints were used, the curved morphology of the radicle could not be sufficiently represented, resulting in larger length estimation errors. When more than four keypoints were used, annotation complexity and computational cost increased, but the improvement in estimation accuracy was limited. Therefore, the four-keypoint strategy was adopted to balance length estimation accuracy, annotation efficiency and computational efficiency.

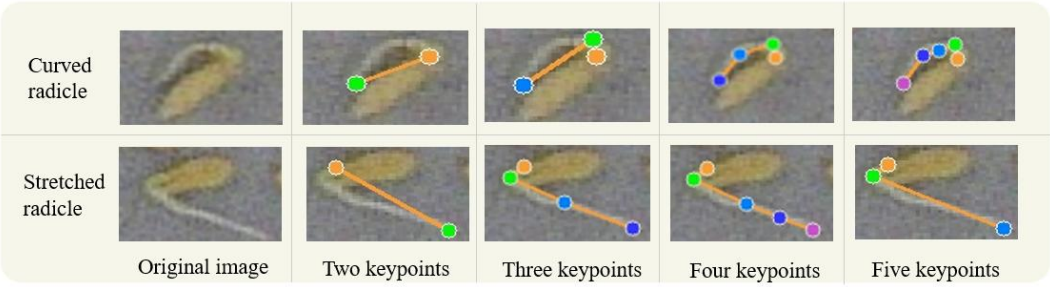

Fig. 3 - Keypoint annotation strategy

Automatic Detection of Individual Cucumber Seeds

To accurately localize individual cucumber seeds in densely distributed Petri dish images, an object detection framework was used as the first step of the proposed method. Germinated cucumber seeds are small and densely distributed, and overlap or partial occlusion may occur among adjacent seeds. Therefore, representative models from different object detection paradigms were selected for comparison, including one-stage detectors, SSD, YOLOv8-p2s, YOLOv8s and YOLO11s; the two-stage detector Faster R-CNN; and the Transformer-based detector DETR.

Each Petri dish image was input into the detection model to obtain the bounding box coordinates and confidence score of each seed instance. The detection results were then used to crop or constrain valid single-seed regions for subsequent radicle keypoint localization. By comparing the detection performance of different models in dense small-object scenarios, the model with the best overall performance was selected as the seed detection module. This step provided accurate spatial priors for radicle keypoint detection and reduced the interference caused by background regions, seed overlap and dense distribution.

Radicle Keypoint Detection Model for Cucumber Seeds

To accurately localize radicle keypoints of individual cucumber seeds, this study proposed a top-down keypoint detection network named GermHRNet. GermHRNet was developed based on HRNet and used HRNet-W32 as the backbone. By maintaining parallel multi-resolution branches throughout the network, the model preserved high-resolution feature representations during feature extraction, which is important for detecting small and slender radicle structures. The overall architecture of GermHRNet is shown in Fig. 4.

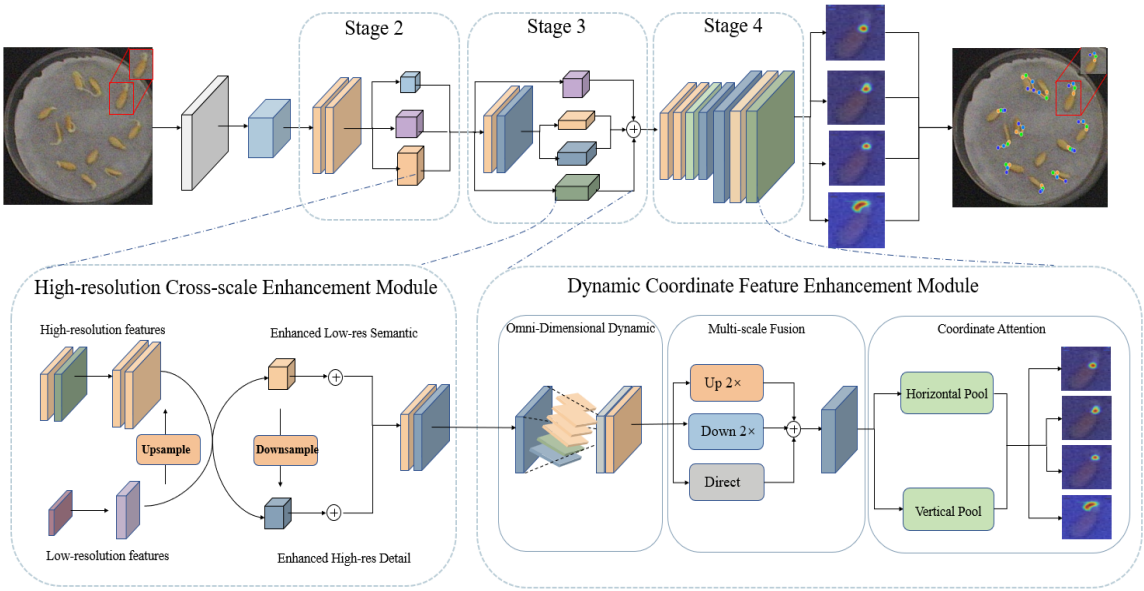

Fig. 4 - Architecture of GermHRNet

To reduce the loss of fine structural information in deeper layers, a High-resolution Cross-scale Enhancement Module (HCEM) was introduced before the multi-scale fusion stage in Stage 3. HCEM maintained the parallel multi-resolution structure of HRNet and established bidirectional cross-scale information pathways. This allowed high-resolution detail features and low-resolution semantic features to interact before fusion, thereby improving the representation of continuous radicle structures and reducing missed keypoint detections.

To further improve localization accuracy, a Dynamic Coordinate Feature Enhancement Module (DCFE) was incorporated into Stage 4. DCFE combined omni-dimensional dynamic convolution blocks, multi-scale feature fusion and coordinate attention. The dynamic convolution blocks adaptively enhanced feature representation according to radicle morphology, while the coordinate attention mechanism introduced directional positional information to guide the network toward key regions such as root tips and bending points. With these designs, the proposed network improved the stability and accuracy of keypoint localization for curved radicles and reduced localization errors caused by complex radicle poses.

High-Resolution Cross-Scale Enhancement Module (HCEM)

Built upon HRNet, a High-Resolution Cross-Scale Enhancement Module (HCEM) is introduced prior to the multi-scale fusion stage (Stage 3). The architecture of HCEM is shown in Fig. 5.

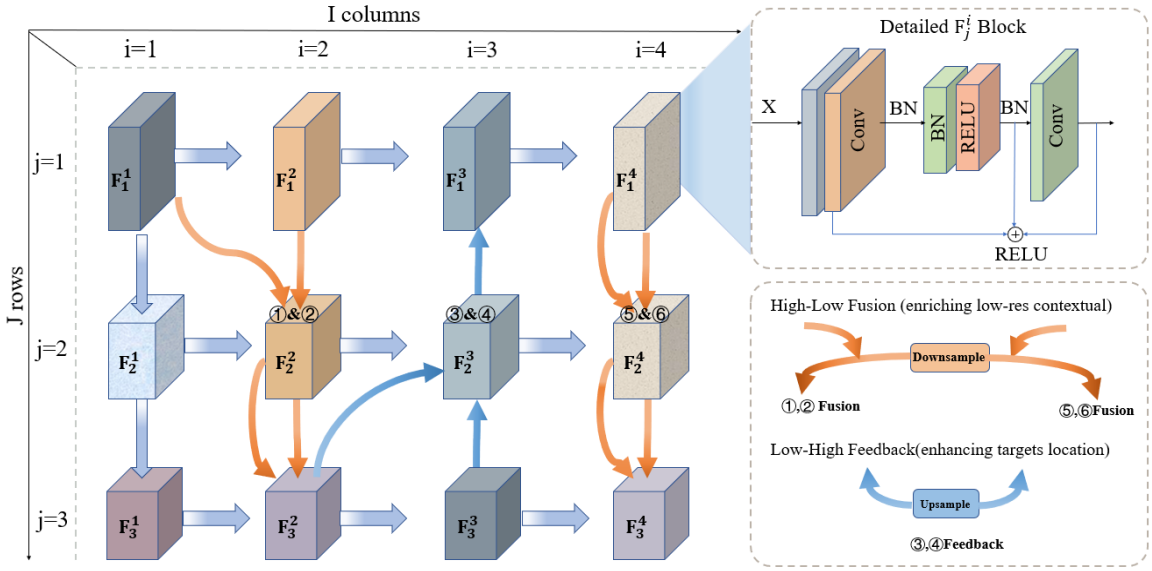

Fig. 5 - Architecture of the High-Resolution Cross-scale Enhancement Module

Considering that the slender and continuous radicle structure depends heavily on spatial resolution and fine-grained details, repeated downsampling leads to reduced spatial resolution and loss of fine-grained information *(Ni et al., 2025)*, thereby affecting the localization of critical radicle regions. Within a parallel multi-resolution framework, the module is organized as a grid-structured network composed of basic residual blocks arranged in i columns and j rows. For the output node F_i^j at the i-th column and j-th row, the computation is defined as follows.

$$F_i^j = X + ReLU\left(BN\left(Conv_2\left(ReLU(BN(Conv_1(X)))\right)\right)\right) \quad (1)$$

where X denotes the input feature map, $Conv_1$ and $Conv_2$ represent two consecutive convolutional layers, BN denotes batch normalization, and $ReLU$ represents the activation function. This structure employs two consecutive convolutional layers with a residual connection, enabling the extraction of discriminative local features while alleviating the vanishing-gradient problem and preserving spatial information.

To enhance feature interaction across different resolution branches, HCEM constructs a bidirectional cross-scale information flow. At even-column nodes, such as nodes ①, ②, ⑤ and ⑥, high-resolution features are downsampled using convolutional operators with a stride of 2 and injected into lower-resolution branches. This process introduces fine-grained spatial cues and alleviates localization ambiguity in low-resolution features caused by enlarged receptive fields. At odd-column nodes, such as nodes ③ and ④, global contextual information from low-resolution branches is upsampled using nearest-neighbor interpolation and propagated to high-resolution branches. This process provides global structural guidance, enabling the network to infer keypoint locations more accurately under radicle bending conditions.

Therefore, HCEM improves the complementarity between high-resolution spatial details and low-resolution semantic context, thereby enhancing the localization accuracy of slender and curved radicles.

Dynamic Coordinate Feature Enhancement Module (DCFE)

Based on HRNet, a Dynamic Coordinate Feature Enhancement Module (DCFE) was introduced in Stage 4. This module was designed to reduce keypoint displacement caused by morphological variations of radicles through joint feature enhancement across spatial, channel and scale dimensions. DCFE consists of three components: an Omni-dimensional Dynamic Block (OD Block), a multi-scale feature fusion module and a Coordinate Attention (CA) module. The overall structure is illustrated in Fig. 6.

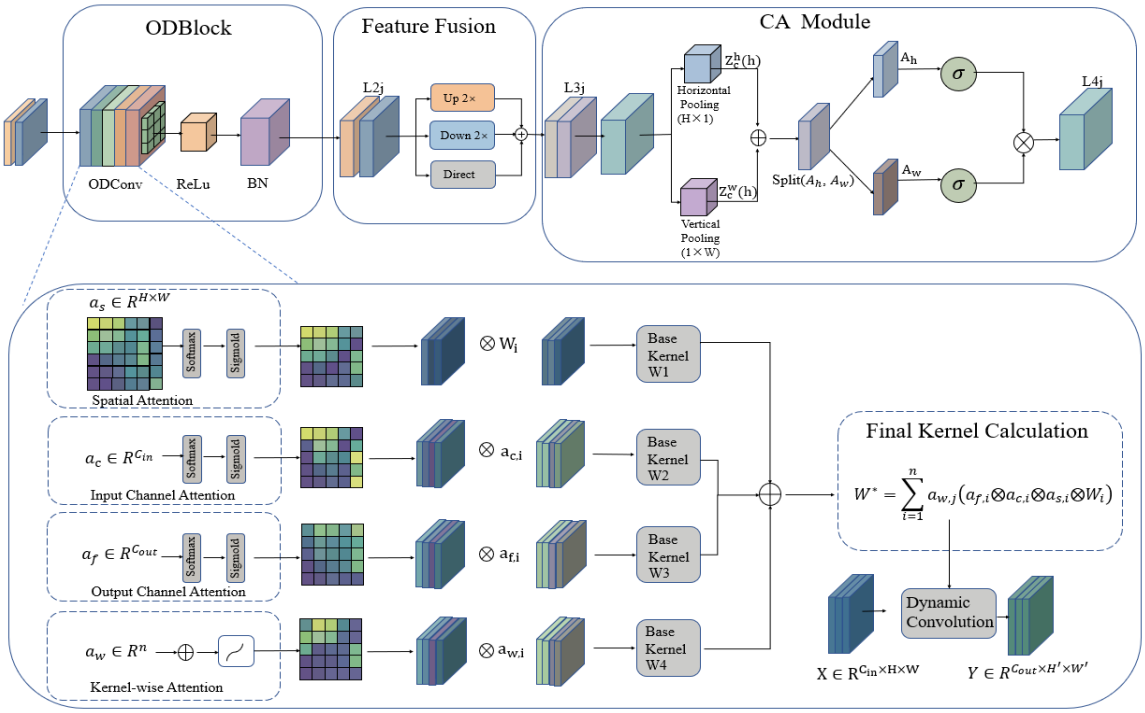

Fig. 6 - Architecture of the Dynamic Coordinate Feature Enhancement Module

The OD Block generates adaptively modulated dynamic convolution kernels based on the contextual information of the input feature map X, enabling the network to adjust feature responses according to radicle morphology. The output Y can be expressed as:

$$\mathrm{Y} = W^*(X) * X \tag{2}$$

where $W^*(X)$ denotes the dynamically generated convolution kernel conditioned on the input feature map X, and $*$ represents the convolution operation. This process performs weighted aggregation of a base kernel pool across four attention dimensions: spatial attention $\mathrm{a_s} \in \mathrm{R^{H\times W}}$ captures pixel-level features of local radicle morphology; input channel attention $\mathrm{a_c} \in \mathrm{R^{C_{in}}}$ and output channel attention $\mathrm{a_f} \in \mathrm{R^{C_{out}}}$ dynamically select the most relevant feature channels for keypoint localization; and kernel−wise attention $\mathrm{a_w} \in \mathrm{R^n}$ enables nonlinear combinations of base kernels. The resulting dynamic convolution kernel is calculated as follows:

$$W^* = \sum_{i=1}^{n} a_{w,i}\left(a_{f,i} \otimes a_{c,i} \otimes a_{s,i} \otimes W_i\right) \tag{3}$$

where W_i denotes the $i-$th base convolution kernel, n is the number of base kernels, and $\otimes$ multi-scale feature fusion module aligns features at different scales by applying upsampling and denotes element-wise multiplication with broadcasting when necessary. This omni-dimensional parameter modulation enables the network to adaptively adjust the receptive field and response intensity of convolutional operators according to different degrees of radicle curvature.

The multi-scale feature fusion module aligns features at different scales by applying upsampling and downsampling operations to the input feature $L_{2,j}$ followed by feature aggregation. This process combines fine-grained spatial details and semantic information, providing a more discriminative feature representation for radicle keypoint localization.

To further enhance spatial positional encoding, a coordinate attention mechanism was incorporated. First, pooling kernels with sizes of (H,1) and (1,W) were used to aggregate spatial information along the horizontal and vertical directions, respectively:

$$Z_c^h(h) = \frac{1}{W}\sum_{0\le i<W} X_c(h,i), Z_c^w(w) = \frac{1}{H}\sum_{0\le j<H} X_c(j,w) \quad (4)$$

where $Z_c^h(h)$ and $Z_c^w(w)$ denote the horizontal output at height h and the vertical output at width w for the $c-$th channel, respectively. The terms $\frac{1}{W}$ and $\frac{1}{H}$ are normalization factors representing averaging pooling. Specifically, $\sum X_c(h,i)$ represents accumulation along the width direction, compressing each row into a single value while preserving positional accuracy along the height dimension. Similarly, $\sum X_c(j,w)$ represents accumulation along the height direction, compressing each column into a single value while preserving positional information along the width dimension.

The aggregated feature maps are then concatenated, convolved, and split to generate two independent directional weights A_h and A_w. After Sigmoid activation, these weights are applied as attention masks to the feature map:

$$L_{4j} = X \otimes \sigma(A_h) \otimes \sigma(A_w) \quad (5)$$

where σ denotes the sigmoid activation function.

This module enhances the network's ability to capture keypoints in curved radicle regions and effectively reduces localization errors. By integrating dynamic convolution, multi-scale feature fusion and coordinate attention, DCFE strengthens spatial consistency in critical regions and improves the accuracy and robustness of keypoint localization.

Radicle Length Estimation and Validation Method

In the radicle length estimation stage, the two-dimensional pixel coordinates of the detected keypoints, including the radicle base, bending points and root tip, were first obtained from the keypoint detection results. These keypoints were then connected sequentially along the radicle growth direction to form a central path. The line segments between adjacent keypoints were regarded as piecewise linear approximations of the radicle structure *(Bagchi et al., 2025)*. The Euclidean distance of each segment was calculated to obtain its pixel length, and the total radicle length in pixels was estimated by cumulative summation. The calculation can be expressed as follows:

$$L_{pixel} = \sum_{k=1}^{m-1} \sqrt{(x_{k+1}-x_k)^2 + (y_{k+1}-y_k)^2}$$

where L_{pixel} is the radicle length in pixels, m is the number of detected keypoints, and (x_k, y_k) denotes the pixel coordinate of the $k-$th keypoint.

A pixel-to-millimeter scale factor was calibrated using the reference ruler in the image acquisition system. The radicle length in pixels was then converted into the actual physical length as follows:

$$L_{mm} = L_{pixel} \times S$$

where L_{mm} denotes the estimated radicle length in millimeters, and S represents the calibrated pixel-to-millimeter scale factor. Through this procedure, automatic radicle length estimation was achieved based on the predicted keypoint coordinates.

To validate the effectiveness of the proposed keypoint-based estimation method, the estimated radicle lengths were compared with manually measured ground-truth values. The manual measurements were used as reference values for accuracy evaluation. In addition, to evaluate the efficiency of automated radicle phenotyping, the total inference time of the complete pipeline, including object detection and keypoint detection, was recorded and analyzed. This evaluation was used to assess the high-throughput capability of the proposed method.

Experimental Parameter Settings

During the object detection training stage, the AdamW optimizer was used with an initial learning rate of 0.001 and a weight decay coefficient of 0.0005. The batch size was set to 16, and the model was trained for 300 epochs. Pretrained weights were used for network initialization to accelerate convergence and improve the initial training stability.

Table 1

Experimental environment configuration

Environment	Details
Programming Language	Python 3.10.15
Operating System	Windows 11

Environment	Details
Deep Learning Framework	PyTorch 2.2.2
CUDA Version	11.8
GPU	NVIDIA RTX 4090
CPU	Intel Core i9-14900KF

For keypoint detection training, the Adam optimizer was adopted with an initial learning rate of 0.0001. The batch size was also set to 16, and the model was trained for 300 epochs. Automatic mixed precision (AMP) training was implemented using NVIDIA Apex to accelerate training and reduce GPU memory consumption. The experimental environment is summarized in Table 1.

Evaluation Metrics

In the comparative experiments for seed instance detection, precision (P), recall (R) and mean average precision (mAP) were used as evaluation metrics *(Rana et al., 2026)*. Precision and recall were used to evaluate the correctness and completeness of seed detection, respectively. The mAP was calculated by first computing average precision (AP) at intersection over union (IoU) thresholds ranging from 0.50 to 0.95 in increments of 0.05 and then averaging the AP values across all thresholds. This metric provides a comprehensive assessment of the localization accuracy and detection performance of the object detection models.

In the radicle keypoint detection experiments, average precision (AP), average recall (AR) and percentage of correct keypoints (PCK) were adopted to evaluate model performance *(Duan et al., 2025)*. AP and AR were calculated according to the COCO (Common Objects in Context) keypoint evaluation protocol, with object keypoint similarity (OKS) used to quantify the similarity between predicted and ground-truth keypoints. Both metrics were averaged over OKS thresholds ranging from 0.50 to 0.95 in increments of 0.05 to characterize the overall accuracy and recall of keypoint detection. PCK was calculated using normalized Euclidean distance, with the longer side of the ground-truth bounding box of each target instance used as the normalization reference. The distance threshold coefficient α was set to 0.05 to evaluate keypoint localization accuracy.

In the radicle length estimation and validation experiments, mean absolute error (MAE), root mean square error (RMSE), coefficient of determination (R^2), normalized mean absolute error (nMAE), and normalized root mean square error (nRMSE) were used to quantitatively evaluate estimation accuracy *(Tan et al., 2025)*. MAE and RMSE were used to quantify the absolute errors between the estimated and ground-truth values, whereas R^2 was used to evaluate the goodness of fit between them. The nMAE and nRMSE were calculated by dividing MAE and RMSE, respectively, by the overall mean of the ground-truth radicle lengths and expressing the resulting ratios as percentages. These normalized metrics quantify the estimation errors relative to the actual radicle length.

In the high-throughput validation experiments, throughput (T) was used to evaluate the efficiency of radicle length acquisition *(Poorter et al., 2023)*. Throughput was defined as the number of seeds processed per hour.

RESULTS AND ANALYSIS

Comparative Experiment on Seed Instance Detection

To select the most suitable detector for cucumber seed localization, six object detection models, including YOLOv8-p2s, YOLOv8s, YOLO11s, Faster R-CNN, DETR and SSD, were compared. The quantitative results are shown in Table 2.

Table 2

Comparison of different object detection models

Model	P%	R%	mAP%
YOLOv8-p2s	98.2	97.9	98.3
YOLOv8s	97.4	97.4	97.8
YOLOv11s	98.0	97.7	97.7
Faster R-CNN	94.9	95.6	94.0
DETR	93.2	97.3	95.4
SSD	95.0	95.3	96.1

YOLOv8-p2s achieved the best overall performance, with precision, recall and mAP values of 98.2%, 97.9% and 98.3%, respectively. Compared with YOLOv8s and YOLO11s, the mAP of YOLOv8-p2s increased by 0.5 and 0.6 percentage points, respectively. It also outperformed SSD, DETR and Faster R-CNN by 2.2, 2.9 and 4.3 percentage points in mAP, respectively. These results indicate that YOLOv8-p2s has better localization accuracy and robustness for densely distributed cucumber seeds.

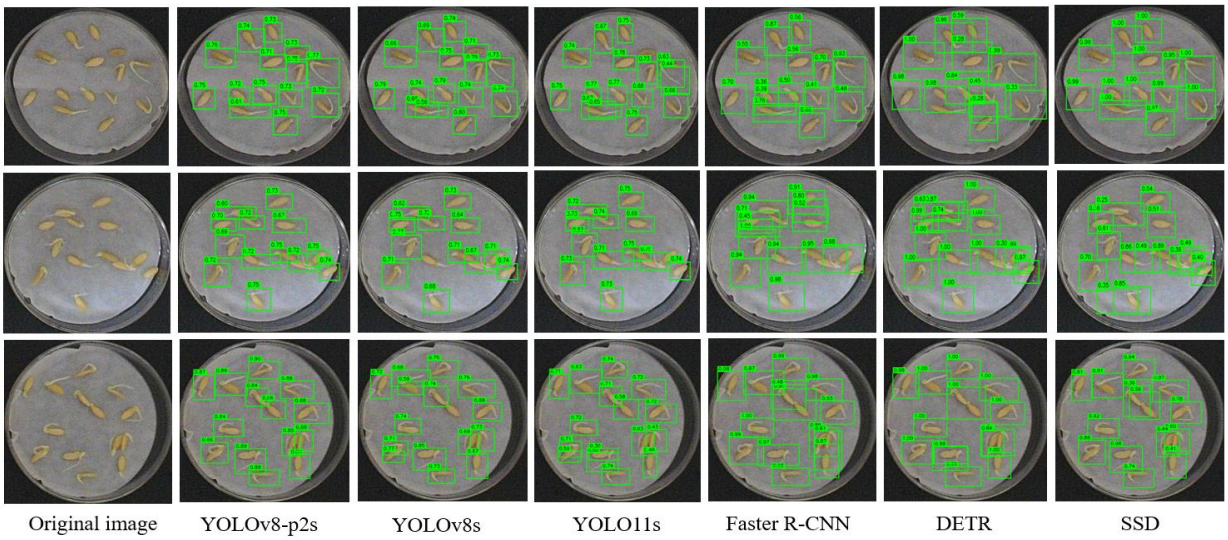

Fig. 7 - Visual comparison of seed instance detection results produced by different object detection models.

Representative detection results are shown in Fig. 7. Under dense small-object conditions, the compared models showed different types of errors, including missed detections, redundant detections and inaccurate localization. YOLOv8s and YOLO11s exhibited missed detections in densely distributed regions, which may be related to the loss of fine-grained features during downsampling. Faster R-CNN tended to generate redundant bounding boxes in crowded regions because of excessive proposal generation. DETR showed limited local detail perception for small targets, resulting in merged detections in clustered regions. SSD produced less accurate bounding boxes, mainly due to insufficient semantic representation in shallow feature maps. In comparison, YOLOv8-p2s produced more compact and accurate bounding boxes by introducing the high-resolution P2 feature layer, which improved the representation of small seed targets and reduced duplicate or missed detections.

Based on the quantitative results and visual comparisons, YOLOv8-p2s was selected as the seed detection model for subsequent radicle keypoint detection and length estimation.

Ablation Study of GermHRNet

To quantitatively evaluate the contributions of the proposed modules, ablation experiments were conducted on the High-resolution Cross-scale Enhancement Module (HCEM) and the Dynamic Coordinate Feature Enhancement Module (DCFE). The performance of each model configuration was evaluated using AP, AR and PCK, as summarized in Table 3.

Table 3

Comparison of ablation experiments with different improvements

Experiment No.	Improvement strategy		AP(%)	AR(%)	PCK(%)
	HCEM	DCFE			
1	×	×	87.5	89.8	86.7
2	√	×	89.6	91.2	87.7
3	×	√	88.7	90.4	87.9
4	√	√	90.6	92.2	88.2

Experiment 1 used the original HRNet as the baseline model, achieving AP, AR and PCK values of 87.5%, 89.8% and 86.7%, respectively. After introducing HCEM in Experiment 2, the AP, AR and PCK increased to 89.6%, 91.2% and 87.7%, respectively, indicating that HCEM enhanced cross-scale feature interaction and improved the structural representation of slender radicles.

In Experiment 3, only DCFE was added to the baseline model, achieving AP, AR and PCK values of 88.7%, 90.4% and 87.9%, respectively. The relatively higher PCK suggests that DCFE improved spatial localization accuracy by enhancing dynamic feature adaptation and coordinate-aware representation, especially for curved regions and root tips.

When both HCEM and DCFE were integrated in Experiment 4, GermHRNet achieved the best performance, with AP, AR and PCK values of 90.6%, 92.2% and 88.2%, respectively. These results show that HCEM and DCFE provide complementary improvements: HCEM strengthens multi-scale structural representation, while DCFE enhances keypoint localization accuracy. Their combination effectively improves the overall accuracy and robustness of radicle keypoint detection.

Comparative Experiment of GermHRNet

To comprehensively evaluate the effectiveness of the proposed GermHRNet, it was compared with five representative keypoint detection methods, namely HRNet, RTMPose, UDP, ViTPose and SimplePose. AP, AR and PCK were used as evaluation metrics, and the quantitative results are presented in Table 4.

Table 4

Comparison of different radicle keypoint detection models

Model	AP(%)	AR(%)	PCK(%)
GermHRNet	90.6	92.2	88.2
HRNet	87.5	89.8	86.7
RTMPose	88.1	90.2	85.0
ViTPose	87.4	90.0	85.4
UDP	86.7	89.3	86.1
SimplePose	86.0	89.2	86.4

As shown in Table 4, GermHRNet achieved the best performance across all evaluation metrics. Compared with the baseline HRNet, GermHRNet improved AP, AR and PCK by 3.1, 2.4 and 1.5 percentage points, respectively. Compared with other representative methods, GermHRNet also consistently outperformed RTMPose, ViTPose, UDP and SimplePose. Specifically, compared with RTMPose, GermHRNet improved AP, AR and PCK by 2.5, 2.0 and 3.2 percentage points, respectively. Compared with ViTPose, the corresponding improvements were 3.2, 2.2 and 2.8 percentage points. Compared with UDP, the improvements were 3.9, 2.9 and 2.1 percentage points. Compared with SimplePose, the improvements reached 4.6, 3.0 and 1.8 percentage points, respectively.

These consistent improvements across multiple metrics indicate that the proposed model has better keypoint detection performance for germinated cucumber seed radicles. In particular, the improvement in PCK suggests enhanced spatial localization accuracy, which is essential for accurately capturing complex radicle structures. Therefore, GermHRNet provided more accurate and stable keypoint localization, especially under challenging conditions involving curved radicles, blurred root tips and densely distributed seeds.

To further evaluate the qualitative performance of different methods, representative visualization results are shown in Fig. 8. Existing methods exhibited several types of errors, including keypoint displacement in curved regions, inaccurate localization of root tips, and redundant or missing detections in densely distributed seed regions. CNN-based methods, such as HRNet and SimplePose, showed localization deviations in some cases, which may be related to the loss of fine spatial details caused by repeated downsampling. ViTPose demonstrated strong global modeling capability, but it still showed limitations in capturing fine-grained local structures of slender radicles. RTMPose and UDP improved coordinate regression or decoding strategies; however, their feature representation ability was still insufficient for accurately modeling complex radicle morphology. In contrast, GermHRNet alleviated these problems by integrating cross-scale feature enhancement and dynamic coordinate-aware representation. The proposed HCEM improved structural continuity through bidirectional multi-scale feature interaction, while DCFE enhanced spatial localization accuracy through dynamic convolution and coordinate attention. As a result, GermHRNet produced keypoint predictions that were more consistent with the actual radicle morphology, particularly in challenging regions such as bending points and root tips.

Overall, both quantitative and qualitative results demonstrate that GermHRNet improves the accuracy and robustness of radicle keypoint localization, validating the effectiveness of the proposed architecture.

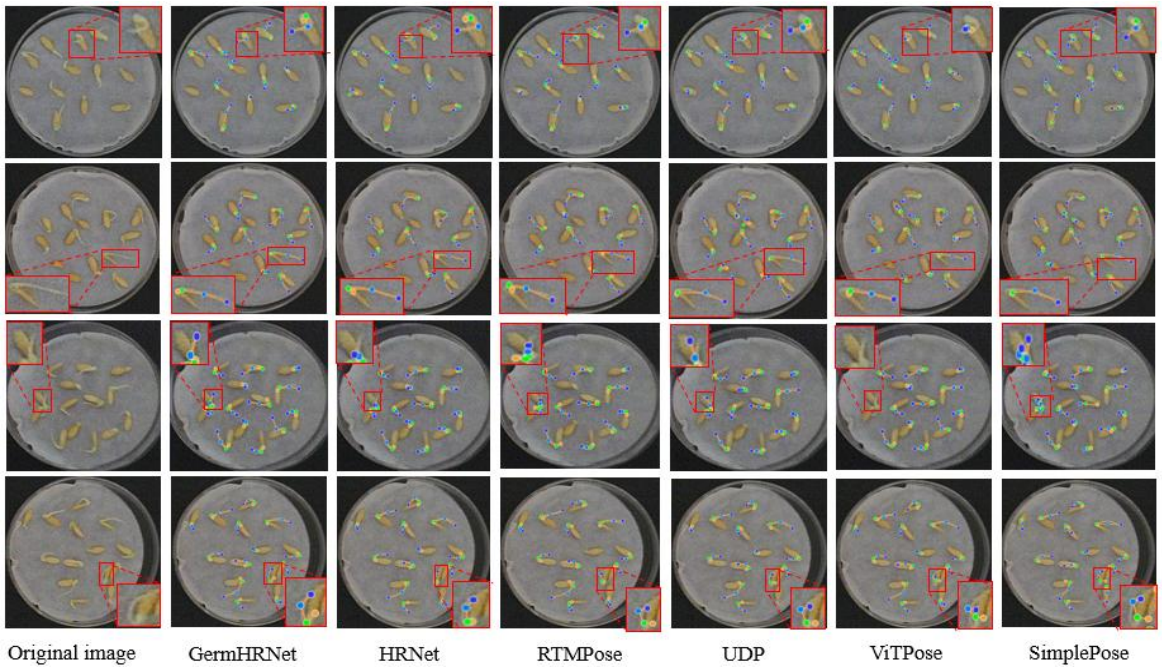

Fig. 8 - Keypoint detection results of germinated cucumber seeds using different models

Radicle Length Validation Experiment

To evaluate the accuracy of GermHRNet for automatic radicle length estimation, a quantitative validation experiment was conducted on all germinated seeds contained in the 120 test-set images. The ground-truth radicle lengths were obtained as follows. First, two experimenters manually measured the radicles corresponding to all seeds in the 120 images using a vernier caliper with a precision of 0.1 mm. Curved radicles were carefully straightened before measurement to obtain their full lengths. Subsequently, a third experimenter reviewed and confirmed all measurement results, and the final confirmed values were used as the ground-truth radicle lengths.

The distribution of the ground-truth radicle lengths in the test set was then statistically analyzed. The mean radicle length was 8.41 mm, with a standard deviation of 4.06 mm. The median was 7.92 mm, and the values ranged from 1.50 to 20.65 mm. This distribution included cucumber seed samples at different degrees of germination, indicating that the test set adequately represented variations in radicle growth during the germination process.

To comprehensively evaluate the overall estimation performance, the error metrics were subsequently calculated. The results showed that the MAE, RMSE, and R^2 were 0.51 mm, 0.61 mm, and 0.98, respectively. As shown in Fig. 9, the data points in the regression plot were closely distributed around the reference line (y=x), indicating strong agreement between the estimated and ground-truth values and a relatively low overall estimation error.

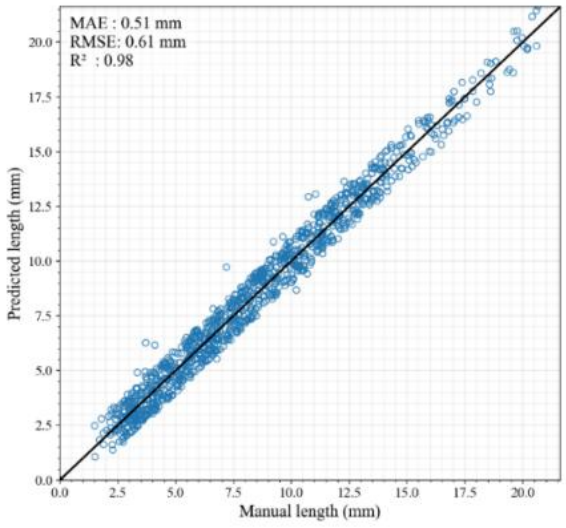

Fig. 9 - Regression analysis of predicted versus ground-truth radicle lengths

To further quantify the relative magnitude of the estimation errors, normalized error metrics were calculated using the mean ground-truth radicle length of 8.41 mm as the normalization reference. The nMAE and nRMSE were 6.06% and 7.25%, respectively. These results indicate that the estimation errors accounted for only a small proportion of the mean ground-truth radicle length, further demonstrating the high accuracy of GermHRNet for automatic radicle length estimation.

Throughput Validation Experiment

To validate the high-throughput processing capability and computational stability of the proposed radicle length estimation method, 120 original images from the CucumberSeeds-2 dataset were used for experimentation. These images contained a total of 19,140 germinated cucumber seeds. The dataset was randomly divided into 10 independent experimental groups, with each group containing 12 original images. All experiments were conducted on a CPU-only platform without GPU acceleration. The hardware configuration is shown in Table 5.

Table 5

Hardware configuration for CPU-only throughput validation

Environment	Details
Programming Language	Python 3.13.2
Operating System	Windows 64-bit (x64)
Memory (RAM)	16 GB
Processor (CPU)	AMD Ryzen 7 7435H (3.10 GHz)

The runtime statistics for the 10 experimental groups are presented in Table 6.

Table 6

Throughput evaluation results of the proposed method under CPU-only conditions

Group No	Seeds Per Original Image	Prep. [s]	Det. [s]	Kpt. [s]	Len [s]	Total [s]	T [seeds/s]
1	175	0.20	0.88	17.31	0.12	18.51	9.45
2	166	0.23	0.86	16.52	0.11	17.72	9.37
3	167	0.23	0.86	16.55	0.11	17.75	9.41
4	160	0.24	0.83	16.01	0.11	17.19	9.31
5	165	0.22	0.79	16.35	0.11	17.47	9.44
6	162	0.21	0.84	16.16	0.11	17.32	9.35
7	150	0.22	0.81	14.93	0.10	16.06	9.34
8	150	0.22	0.85	14.84	0.10	16.01	9.37
9	149	0.20	0.81	14.80	0.10	15.91	9.37
10	151	0.24	0.82	14.97	0.10	16.13	9.36

Each group contained 12 original images, and the reported time values were averaged per original image within each group. Abbreviations: Prep. = image preprocessing time; Det. = object detection time; Kpt. = keypoint detection time; Len. = radicle length estimation time; Total = total processing time per original image; T = throughput, expressed as seeds per second.

As shown in Table 6, the average processing time per original image ranged from 15.91 s to 18.51 s, with an overall mean of approximately 17.01 s. The relatively small variation in processing time indicates good computational stability of the entire pipeline under different seed densities. Among all processing steps, keypoint detection accounted for the largest proportion of the total processing time, whereas image preprocessing, object detection and length estimation required relatively short computation times.

Based on the average throughput across the 10 experimental groups, the proposed system achieved a processing capacity of approximately 3.38×10^4 seeds/h on a single machine. Compared with manual measurement, which processes approximately 120 seeds/h, the proposed method substantially improved radicle length acquisition efficiency. These results demonstrate that the proposed method has strong high-throughput processing capability and is suitable for large-scale cucumber seed phenotyping and microbial strain screening.

CONCLUSIONS

To address the limitations of low efficiency, subjective measurement errors and insufficient throughput in germination tests for plant growth-promoting rhizobacteria (PGPR) screening, this study proposed an automatic radicle length estimation method for germinated cucumber seeds based on GermHRNet. The proposed framework achieved automated analysis from seed localization and radicle keypoint detection to radicle length quantification. The main conclusions are as follows.

1) A GermHRNet-based keypoint detection network for germinated cucumber seed radicles was developed. To improve feature representation for slender and curved radicle structures, cross-scale feature enhancement and coordinate-aware dynamic feature modeling strategies were incorporated into the HRNet backbone. The proposed model achieved AP, AR and PCK values of 90.6%, 92.2% and 88.2%, respectively, outperforming the compared mainstream keypoint detection models. These results demonstrate that the proposed framework improved the accuracy and robustness of radicle keypoint localization under complex morphological conditions.

2) A polyline-based radicle length estimation strategy was proposed for curved radicle estimation. Based on the detected keypoint coordinates, radicle length was estimated through multi-segment polyline pixel accumulation. The proposed method achieved MAE, RMSE, nMAE, nRMSE, and R^2 values of 0.51 mm, 0.61 mm, 6.06%, 7.25%, and 0.98, respectively, showing strong agreement with manual measurements. These results indicate that the proposed method can satisfy the accuracy requirements of radicle phenotyping and seed vigor evaluation.

3) The proposed method demonstrated strong high-throughput processing capability. Throughput experiments showed that the proposed framework achieved a processing capacity of approximately 3.38×10^4 seeds/h on a CPU-only platform. Compared with manual measurement (~120 seeds/h), the proposed method improved radicle length acquisition efficiency by approximately 282-fold. These results demonstrate the practical potential of the proposed framework for large-scale cucumber seed phenotyping and PGPR screening applications.

Although GermHRNet achieved favorable performance in radicle keypoint detection and automatic length estimation for germinated cucumber seeds, several limitations remain. First, the experiments were limited to seeds from a single cucumber cultivar and a specific germination stage. Further investigation is therefore required to determine how variations in radicle morphology across different cultivars and germination stages affect keypoint detection and length estimation performance. Second, all experimental data were acquired using a single imaging system under controlled laboratory conditions. Consequently, the generalizability of the model across different imaging devices and illumination conditions has not yet been fully validated.

To address these limitations, future studies will conduct external validation using different cucumber cultivars, germination stages, and imaging conditions to further assess the robustness and applicability of the model. In addition, lightweight deployment and real-time integration of the proposed framework with image acquisition systems will be further investigated to improve computational efficiency and system stability, thereby providing a more efficient and reliable solution for high-throughput and standardized seed phenotyping.

ACKNOWLEDGEMENT

This research was funded by the Potato Innovation Program for the Chief Expert of Shandong Province (Grant No. SDAIT-16-01).

REFERENCES

[1] Bagchi, P., Seredin, O. S., Kopylov, A. V., Surkov, E. E., Mityugov, N. S., Tokarev, A. R., & Bhattacharjee, D. (2025). Skeletons distance evaluation for automated control of exercises in physical therapy. *The International Archives of the Photogrammetry, Remote Sensing and Spatial Information Sciences*, XLVIII-2/W9-2025, 33–38. https://doi.org/10.5194/isprs-archives-XLVIII-2-W9-2025-33-2025

[2] Chen, H., Song, Q., Chang, T., Zheng, L., Zhu, X., Zhang, M., et al. (2024). Extraction of single-tiller rice phenotypic parameters based on YOLOv5m and CBAM-CPN. *Transactions of the Chinese Society of Agricultural Engineering,* 40(2), 307–314. https://doi.org/10.11975/j.issn.1002-6819.202304126

[3] Chen, P., Yan, B., Deng, G., Li, G., Cui, Z., Zheng, S., et al. (2025). Pose detection and localization of pineapple fruit picking based on improved LiteHRNet. *Frontiers in Plant Science*, 16, 1577312. https://doi.org/10.3389/fpls.2025.1577312

[4] Duan, W., Wang, F., Li, H., et al. (2025). Lameness detection in dairy cows from overhead view: High-precision keypoint localization and multi-feature fusion classification. *Frontiers in Veterinary Science*, 12, 1675181. https://doi.org/10.3389/fvets.2025.1675181

[5] Fu, Y., Lin, K., Cheng, B., Qi, L., Zhang, Q., Li, H., Chen, X., & Zhang, C. (2026). Phosphate-solubilizing Bacillus subtilis Y31 promotes cucumber growth and yield: insights from rhizosphere microbiomics and bacterial genomics. *Frontiers in Microbiology*, 16, 1751005. https://doi.org/10.3389/fmicb.2025.1751005

[6] He, J., Weng, L., Xu, X., Chen, R., Peng, B., Li, N., et al. (2024). DEKR-SPrior: An efficient bottom-up keypoint detection model for accurate pod phenotyping in soybean. *Plant Phenomics,* 6, 0198. https://doi.org/10.34133/plantphenomics.0198

[7] Hu, T., Shen, P., Zhang, Y., et al. (2025). OpenPheno: An open-access, user-friendly, and smartphone-based software platform for instant plant phenotyping. *Plant Methods*, 21, 76. https://doi.org/10.1186/s13007-025-01395-4

[8] Li, J., Lu, J., Liu, L., & Wang, K. (2026). UAV-based high-throughput phenotyping of soybean using lightweight point detection for multi-organ trait extraction. *INMATEH-Agricultural Engineering*, 78(1), 410-421. https://doi.org/10.35633/inmateh-78-33

[9] Ni, R., et al. (2025). Point-to-point regression: Accurate infrared small target detection with single-point annotation. *IEEE Transactions on Geoscience and Remote Sensing*, 63, 5002719. https://doi.org/10.1109/TGRS.2025.3554025

[10] Niu, Z., & Qiu, Z. (2025). Extraction method of maize plant skeleton and phenotypic parameters based on improved YOLOv11-Pose. *Smart Agriculture,* 7(2), 95–105. https://doi.org/10.12133/j.smartag.SA202501001

[11] Pan, Y., Chang, J., Dong, Z., Liu, X., & Li, H. (2025). PFLO: A high-throughput pose estimation model for field maize based on YOLO architecture. *Plant Methods, 21*, 51. https://doi.org/10.1186/s13007-025-01369-6

[12] Poorter, H., Hummel, G. M., Nagel, K. A., Fiorani, F., von Gillhaussen, P., Virnich, O., Schurr, U., Postma, J. A., van de Zedde, R., & Wiese-Klinkenberg, A. (2023). Pitfalls and potential of high-throughput plant phenotyping platforms. *Frontiers in Plant Science, 14*, 1233794. https://doi.org/10.3389/fpls.2023.1233794

[13] Rana, A., & Vaidya, P. (2026). YOLO-based deep learning framework for real-time multi-class plant health monitoring in precision agriculture. *Scientific Reports, 16*(1), 197. https://doi.org/10.1038/s41598-025-29132-w

[14] Shaik, A., Karthikeyan, R., & Kousik, C. S. (2025). Growth stage-specific responses of cucumber to salinity stress: Germination, seedling establishment, and vegetative development. *Frontiers in Plant Science, 16*, 1617809. https://doi.org/10.3389/fpls.2025.1617809

[15] Tan, Z., Xiao, D., Liu, J., et al. (2025). Cascade vision-based weight estimation algorithm for monitoring fattening pig weight. *Computers and Electronics in Agriculture, 236*, 110384. https://doi.org/10.1016/j.compag.2025.110384

[16] Top Cloud-Agri Technology Co., Ltd. (2026). *TPN-Pheno-ZM1 in situ root phenotyping system for seed germination stage*. Retrieved April 23, 2026, from https://www.tpyn.net/productshow_615.html

[17] Wu, Y., Li, Z., Jiang, H., Li, Q., Qiao, J., Pan, F., Fu, X., & Guo, B. (2024). YOLOv8-segANDcal: Segmentation, extraction, and calculation of soybean radicle features. *Frontiers in Plant Science, 15*, 1425100. https://doi.org/10.3389/fpls.2024.1425100

[18] Wu, Z., Xia, F., Zhou, S., & Xu, D. (2023). A method for identifying grape stems using keypoints. *Computers and Electronics in Agriculture, 209*, 107825. https://doi.org/10.1016/j.compag.2023.107825

[19] Yuan, C., Zhao, Z., Huang, X., Hu, Z., & Chen, R. (2026). Phalaenopsis flower stem length measurement method based on keypoint detection. *Measurement, 271*, 120865. https://doi.org/10.1016/j.measurement.2026.120865

[20] Zhao, J., Hou, Z., Hua, H., Nie, Q., Pang, Y., Ma, Y., & Huang, X. (2025). LenRuler: A rice-centric method for automated radicle length measurement with multicrop validation. *Plant Phenomics,* 7(3), 100103. https://doi.org/10.1016/j.plaphe.2025.100103